



Article

## Beyond Shade Provision: Pedestrians' Visual Perception of Street Tree Canopy Structure Characteristics in Guangzhou City, China

Jiawei Wang 1,2, Jie Hu 1,2 and Yuan Ma 1,2,\*

- School of Architecture and Urban Planning, Guangdong University of Technology, Guangzhou 510090, China; 2112310080@mail2.gdut.edu.cn (J.W.); 13420533536@mails.gdut.edu.cn (J.H.)
- <sup>2</sup> Landscape Planning and Ecological Restoration Research Center, Guangdong University of Technology, Guangzhou 510090, China
- \* Correspondence: mayuan@gdut.edu.cn

#### **Abstract**

This study examines the impact of canopy structural characteristics on pedestrians' visual perception and psychophysiological responses along four roads in the subtropical city of Guangzhou: Huadi Avenue, Jixiang Road, Yuejiang Middle Road, and Huan Dao Road. A Canopy Structural Index (CSI) was innovatively developed by integrating tree height, crown width, diffuse non-interceptance, and leaf area index, establishing a five-tier quantitative grading system. The study used multimodal data fusion techniques combined with heart rate variability (HRV) analysis and eye-tracking experiments to quantitatively decipher the patterns of autonomic nervous regulation and visual attention allocation under different levels of CSI. The results demonstrate that CSI levels are significantly correlated with psychological relaxation states: as CSI levels increase, time-domain HRV metrics (SDNN and RMSSD) rise by 15%-43%, while the frequency-domain metric (LF/HF) decreases by 31%, indicating enhanced parasympathetic activity and a transition from stress to relaxation. Concurrently, the allocation of visual attention toward canopies intensifies. The proportion of fixation duration increases to nearly 50%, and the duration of the first fixation extends by 0.3–0.8 s. The study proposes CSI  $\leq$  0.15 as an optimization threshold, offering scientific guidance for designing and pruning subtropical urban street tree canopies.

Keywords: eye movement; canopy; HRV; CSI; physiology; healthy environment



Academic Editor: Hiroaki Ishii

Received: 11 August 2025 Revised: 8 October 2025 Accepted: 11 October 2025 Published: 13 October 2025

Citation: Wang, J.; Hu, J.; Ma, Y. Beyond Shade Provision: Pedestrians' Visual Perception of Street Tree Canopy Structure Characteristics in Guangzhou City, China. Forests 2025, 16, 1576. https://doi.org/10.3390/ f16101576

Copyright: © 2025 by the authors. Licensee MDPI, Basel, Switzerland. This article is an open access article distributed under the terms and conditions of the Creative Commons Attribution (CC BY) license (https://creativecommons.org/licenses/by/4.0/).

## 1. Introduction

Urban street trees, as a core component of green infrastructure, have garnered widespread attention for their ecological and aesthetic benefits [1]. However, previous studies have emphasized their ecological functions, such as carbon sequestration and oxygen release [2], microclimate regulation [3], cooling and dust retention [3], and stormwater interception [2], while research on how canopy structural characteristics influence pedestrian visual perception remains limited. As the "Healthy Cities" concept has deepened, the regulatory role of the visual perception of built environments on human psychophysiology has gradually become a cross-disciplinary research focus in environmental psychology and landscape architecture [4]. Wang Beibei et al. [5] investigated the activity times of adults engaged in indoor and outdoor activities across 31 provinces in China through questionnaires. The results indicated that Chinese residents spend 3–4 h daily on outdoor activities, highlighting the importance of visual contact with urban greenery. The following pictures show the distribution of street trees in the city (Figure 1).

Forests 2025, 16, 1576 2 of 25

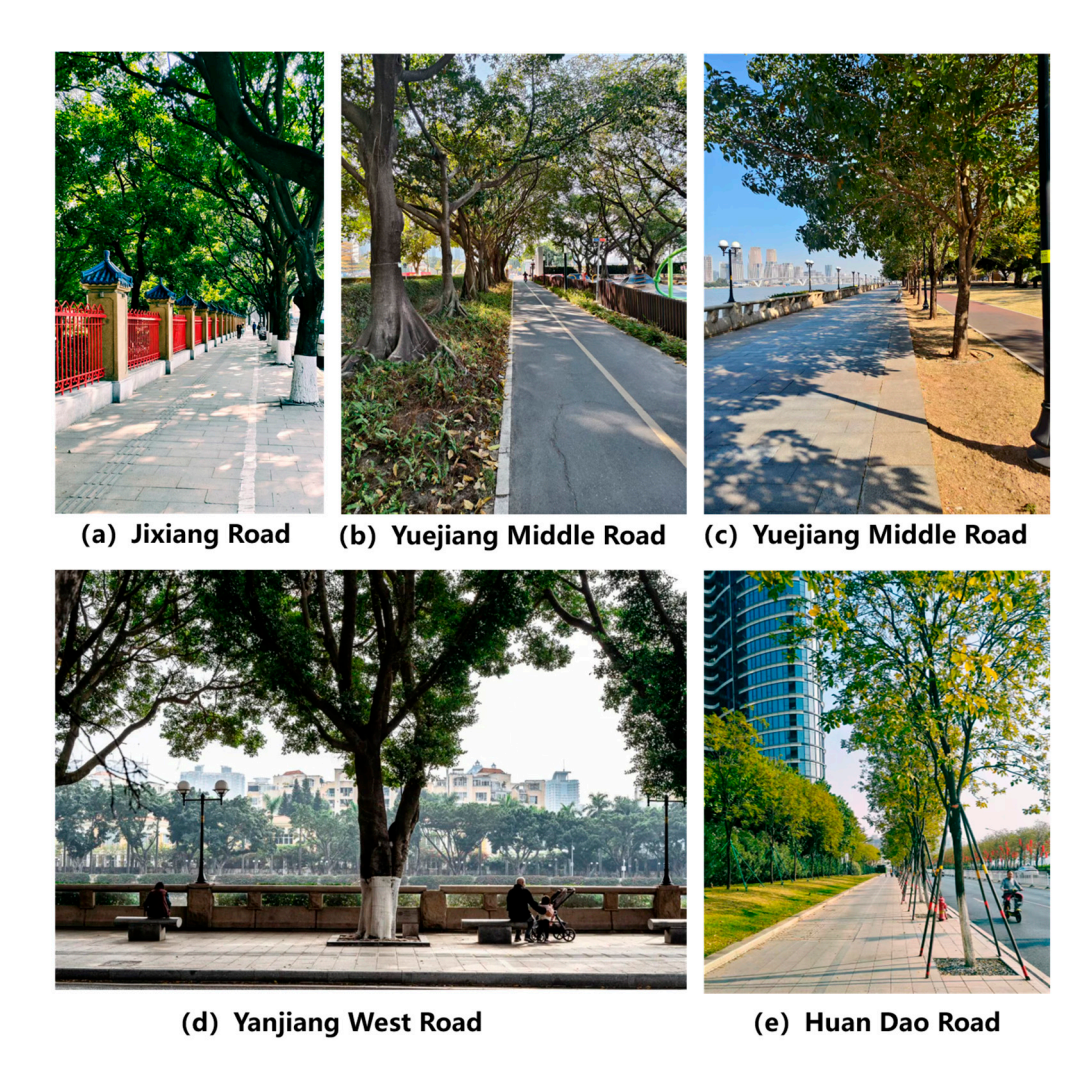


**Figure 1.** Street trees in the city.

To advance research on how canopy structural characteristics influence pedestrians' visual perception, we explored whether integrating specific tree canopy metrics could establish a new composite indicator for analyzing the quantitative relationships between canopy structural features and psychophysiological responses of pedestrians. Specifically, we hypothesized that:

- (1) Is there a specific level of the canopy structural index at which pedestrians become mentally more excited and prefer walking on such streets?
- (2) Is there a specific canopy structural index level at which pedestrians shift their visual attention allocation toward canopy areas, becoming visually captivated by the canopy?

#### 1.1. The Interaction Mechanism Between the Canopy Structure and the Visual Environment

Pedestrian visual perception is a core dimension of evaluating urban spatial quality, encompassing metrics such as the green view index, visual openness, and spatial coherence [6]. Recent advances in multidisciplinary approaches, such as streetscape image analysis and virtual reality simulation, have provided new pathways for quantifying visual perception. For instance, J. Han et al. [7] found through immersive VR combined with eyetracking experiments that when the street green view index was  $\geq$ 18% and sky openness was  $\geq$ 30%, ratings for "naturalness" and "aesthetic appeal" significantly increased by 60%; simultaneously, a shade coverage ratio  $\geq$  20% boosted pedestrians' willingness to linger by 50%. However, canopy structures have a dual effect on visual perception: moderate green view rates alleviate visual fatigue and reduce anxiety, whereas excessive density may

Forests 2025, 16, 1576 3 of 25

obstruct skylines and induce feelings of oppression [8]. In an empirical study in Shanghai, Shao Yuhan et al. [8] further indicated that the ideal green view index-to-openness ratio varies with street orientation. The GVI/SVI ratio should be 1:1.2 for north-south streets, but it should be adjusted to 1:1.5 for east-west streets to avoid "tunnel effects". Additionally, canopy light transmittance (CLT) is a key factor: Li Xin et al. [9] demonstrated through deep learning analysis that pedestrian perceived pleasure peaks at CLT levels of 20%–30%; values below 10% or above 50% may cause glare or visual monotony. Li et al. further supported this in VR eye-tracking experiments. They found that high canopy density significantly increased pupil diameter, suggesting an elevated visual load [10].

#### 1.2. Technological Breakthrough in Multimodal Perceptual Measurement

Recent advancements in multimodal perceptual measurement technologies have revolutionized our understanding of urban landscapes. Previously, studies relied heavily on subjective questionnaires or static images, which struggled to capture dynamic human responses in real environments [11]. Now, with physiological sensors such as eye trackers, EEG, and GSR devices, researchers can simultaneously record visual behaviors and physiological states, such as gaze movements, heart rate fluctuations, and emotional variations, in real-world settings. This allows them to construct intricate correlation models between physiology, vision, and psychology [12]. For example, the ErgoLAB humanenvironment synchronization platform integrates wearable eye trackers and high-precision sensors to achieve millisecond-level synchronization of visual-emotional data. In a study of Chongqing's mountainous parks, the system revealed a nonlinear relationship ( $R^2 = 0.68$ ) between canopy light transmittance and pupil constriction speed, showing how plant shading instantly affects visual load [12]. Technological progress has also significantly enhanced data reliability. Multimodal eye trackers employ filtering algorithms and neural networks to reduce pupil positioning errors under disruptive conditions (e.g., strong light) from  $\pm 2.5^{\circ}$  to  $\pm 0.7^{\circ}$ , enabling more precise outdoor experiments. These tools have moved beyond laboratories into real streets. For instance, mobile monitoring vehicles in Shanghai utilize lidar and infrared vision devices to assess canopy health and thermal comfort while in motion. Crucially, researchers have identified the preferred canopy light transmittance range (20%–28%) under hot-humid conditions and established quantitative relationships with anxiety by applying machine learning to analyze over 150,000 sets of eye-tracking and physiological data. Collectively, these advancements mark a transition of urban landscape research from "experience-driven" to fully "data-driven" approaches [11]. These multimodal methods are particularly valuable for exploring the influence of tree canopy structural parameters on psychophysiological responses.

#### 1.3. Innovative Framework of the Study

While existing research has demonstrated the positive impacts of green spaces on mental health [13], investigations focusing on street trees—linear landscape elements in urban public spaces—remain limited. This study transcends the constraints of conventional landscape assessment methodologies reliant on subjective questionnaires by establishing a tripartite "physiological-behavioral-environmental" coupling framework for analyzing the effects of canopy perception. The groundbreaking innovations are manifested in two dimensions:

(1) Theoretical Innovation: This research introduces the Canopy Structural Index (CSI) as a standardized metric for quantifying crown spatial morphology. We developed a five-tier classification system (Levels 1–5) by integrating four critical canopy parameters—tree height, crown width, leaf area index (LAI), and Diffusion Non-interceptance—representing a seminal advancement in urban tree canopy characterization. (Figure 2).

Forests 2025, 16, 1576 4 of 25

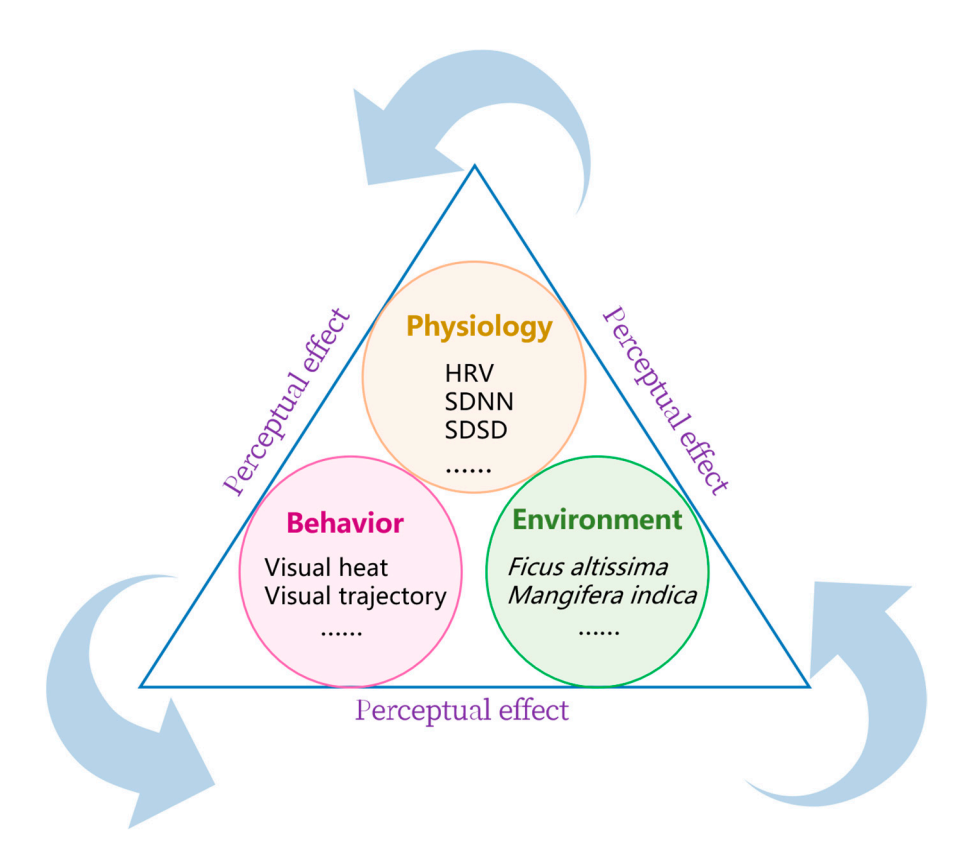


Figure 2. "Physiology-behavior-environment" coupling diagrams.

(2) Methodological Innovation: Employing multimodal data fusion analytics, we systematically integrated objective physiological-behavioral indicators, including heart rate variability (HRV) and eye-tracking fixation heatmaps, to construct a multidimensional dynamic monitoring system. This apparatus precisely captures human perceptual states. Through standardized environmental exposure experiments that controlled for confounding variables, we innovatively elucidated dose-response relationships between CSI levels and autonomic nervous regulation and visual attention allocation.

## 2. Experimental Steps

- 2.1. Canopy Landscape Image
- 2.1.1. Data Collection
  - (1) Street Selection and Panoramic Image Acquisition

The study selects five typical streets along the Pearl River in Guangzhou (Figure 3): Huadi Avenue, Jixiang Road, Yuejiang Middle Road, Yuejiang Middle Road, and Huan Dao Road. Among them, a length of 500 m was selected for sampling, and the traffic flow on these streets is not very high, making them typical pedestrian walkways. The selection of tree species follows dual criteria, namely ecological representativeness, covering the main roadside tree species in subtropical cities, including evergreen broad-leaved trees (Ficus microcarpa), deciduous ornamental trees (Ulmus chinensis), economic fruit trees (mango trees), fast-growing trees (peach blossom trees), and small trees (purple hydrangeas), reflecting the diversity of canopy structure; Spatial distribution frequency: The selected street is in the top five combinations with the highest frequency of tree configuration patterns in high-density built-up areas.

Forests **2025**, 16, 1576 5 of 25

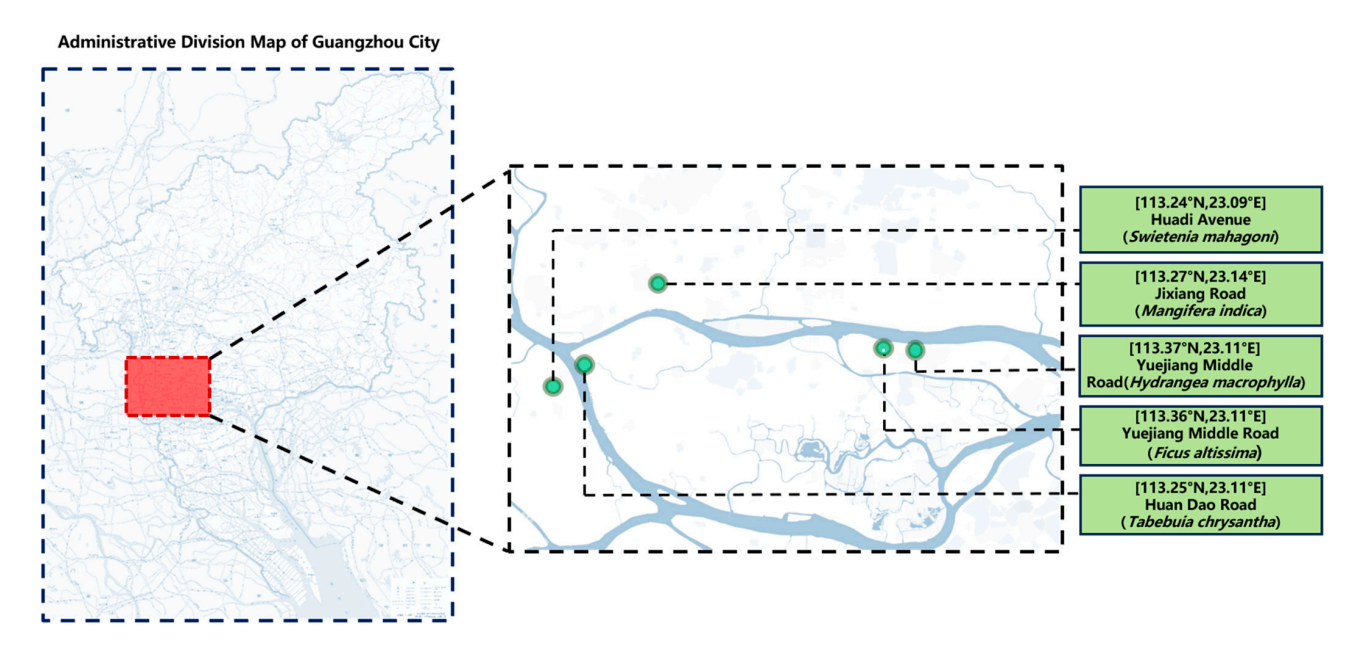


Figure 3. Study the location map.

Image acquisition was conducted during the period of stable leaf area (10–25 February 2025, 10:00–14:00) using an Insta360 Pro 2 panoramic camera following standardized protocols. The acquisition specifications were as follows:

Viewpoint simulation: The camera height was fixed at 1.5 m (simulating the average pedestrian eye level);

Spatial sampling: A 50~m section of each street was selected, with one panoramic photo taken every 15~m;

Environmental control: Real-time monitoring ensured stable thresholds for light intensity, wind speed, temperature, and humidity.

Post-processing: raw images underwent color temperature correction and size standardization, outputting HDR images in the DCI-P3 color gamut, resulting in 15 experimental stimulus materials (Figure 4).



Figure 4. Panoramic image of street trees.

#### (2) Canopy Structural Parameter Acquisition

The DJ-3200 Plant Canopy Analysis System was employed to capture hemispherical canopy images for 10 standard trees on each street. The system was configured with a Sony ILCE-ZV10 camera equipped with a  $180^{\circ}$  fisheye lens and a polarizing filter attached to the

Forests 2025, 16, 1576 6 of 25

front of the lens. During the measurements, the shooting point was set at the base of each (1.5 m above the ground), with the lens's optical axis maintained vertically upward. Each tree was photographed three times repeatedly, and the average value was taken. Two core parameters, DIFN and LAI, were calculated using canopy analysis software.

Additionally, the tree height and crown width were measured using a Leica Disto D2 laser rangefinder. A baseline was established at the vertical projection point of the tree base. The operator held the instrument at a known horizontal distance (L), aimed at the treetop vertex, and recorded the slope distance (S) and elevation angle ( $\alpha$ ). Tree height was calculated using the formula  $H = S \cdot \sin \alpha + h$  (where h is the instrument holding height of the operator), with the process repeated three times to average out aiming errors. The crown width was measured from the center of the tree trunk to determine the edge-to-edge width of the foliage in both the north-south (N-S) and east-west (E-W) directions. CW = (dns + dew)/2 (Table 1).

Index	Index Instrument Brand Manufacturer		Measurement Range	Error	
Illuminance	Illuminance meter	Konica Minolta T-10	Japan: Konica Minolta	0.01~299,900 lux	±2%
Wind speed	Handheld anemometer	DEM6 type three cup anemometer	China: Yiou Instrument Equipment Co., Ltd.	1 m/s~30 m/s	<0.4 m/s
Temperature	Temperature and humidity recorder	JTR08C Temperature and Humidity Recorder	China: Xinrui Instrument Co., Ltd.	−25—40 °C	±0.5 °C
Humidity	Temperature and humidity recorder	JTR08C Temperature and Humidity Recorder	China: Xinrui Instrument Co., Ltd.	20%~80% RH	$\pm 5\%$ RH
Tree height/Crown width	Laser rangefinder	Leica DISTO D2	Germany: Leica	0.05-60 m	$\pm 1.5~\mathrm{mm}$
LAI	Canopy analyzer	DJ3200 Plant Canopy Analysis System	China: DianDian Technology	0.01~20 LAI	±0.03 LAI
DIFN	Canopy analyzer	DJ3200 Plant Canopy Analysis System	China: DianDian Technology	0%-100%	±2%
Photo sphere	Panoramic camera	Insta360 Pro 2	China: Insta		

**Table 1.** Measuring instrument.

#### 2.1.2. Canopy Structural Index (CSI)

To study the influence of street tree canopy structural characteristics on pedestrians' visual perception, this study introduces a new metric—the Canopy Structural Index (CSI)—composed of the following indicators. Tree Height (H): defines the sense of vertical scale in the street space. Moderate tree height can provide a pleasant sense of spatial enclosure, while excessively tall or short trees may induce feelings of oppression or insufficient openness. Crown Width (Cw): determines the coverage extent of the canopy over the street, directly affecting the continuity of shade and the "green canopy" effect of the street. Diffuse Non-interceptance (DIFN): This is a key light environment parameter that quantifies the proportion of diffuse radiation penetrating the canopy. It directly determines the light intensity and the light-shadow ambiance under the trees. A high DIFN value signifies a brighter under-canopy environment. Leaf Area Index (LAI): As a core parameter describing vegetation canopy structure and function, LAI is defined as the ratio of the total leaf area per unit ground area. It directly reflects the luxuriance, or "solid density", of the canopy and is a decisive factor influencing light penetration, ventilation, and the permeability of pedestrians' sightlines. This formula did not conduct statistical model comparison and evaluation, but instead used expert scoring method to analyze the indicators. The formula for the Canopy Structural Index (CSI) is as follows:

$$CSI = \left(\frac{DIFN^{0.7} \cdot H^{0.3}}{LAI^{0.9}}\right) \cdot ln(1 + 0.5Cw) \tag{1}$$

In this formula, the numerator term  $DIFN^{0.7} \cdot H^{0.3}$  represents the "space and brightness" factor that positively influences visual perception. The placement of DIFN and H in the

Forests 2025, 16, 1576 7 of 25

> numerator indicates that higher values of these metrics increase the CSI score. This aligns with common intuitive perception: an under-canopy space that is bright and permeable (high DIFN) while providing sufficient vertical openness (high H) typically evokes more positive, comfortable, and safe visual and psychological experiences. The denominator term LAI<sup>0.9</sup> represents the "density" or "congestion" factor that may negatively affect visual perception. Placing LAI in the denominator reflects its dual nature and potential negative effects on perceptual experience. While a certain degree of LAI is necessary for creating shade, excessively high LAI leads to an overly dense canopy, resulting in an understory environment that is too dark, lacks light-shadow variation, and may even induce feelings of oppression, gloom, or insecurity due to obstructed sightlines. Therefore, placing LAI in the denominator with a high exponent (0.9) ensures that a canopy, regardless of its height (large H) or crown width (large Cw), will yield a correspondingly lower CSI score if it is excessively dense (extremely high LAI), resulting in a dark understory (very low DIFN). This accurately simulates the negative perception associated with an "impenetrable" canopy in the real world. The crown width adjustment term ln(1 + 0.5Cw) models the "law of diminishing marginal effects" for Cw influence. In the urban street environment, the change from having no canopy (e.g., Cw = 0) to having a canopy (e.g., Cw = 4 m) creates a substantial visual impact and significant improvement in spatial perception for pedestrians. However, when a street already has a continuous, 20-m-wide tree canopy, an additional 4-m increase in crown width provides negligible additional perceptual improvement. Using the natural logarithm function ln(1 + x) effectively models this non-linear growth relationship: rapid growth initially, followed by a gradually decreasing growth rate, eventually plateauing. This allows the CSI index to more realistically reflect the marginal contribution of crown width changes to subjective perception under different contexts. Furthermore, CSI is a dimensionless unit. Dimensional effects are eliminated through the normalization of the various physical quantities. This ensures the index can be used for comparing canopy structures across different environments and scales, enhancing its universality.

> Regarding the issue of indicator weights, we invited 10 experts with over 10 years of research experience in environmental psychology, landscape design, urban forestry, and other fields to rate the relative importance of the four parameters (H, Cw, DIFN, LAI) on a scale of 1–9 using the Saaty Analytic Hierarchy Process. Based on the comprehensive expert scoring results, the relative weights of each parameter are calculated and then converted into an exponential form (Table 2).

Parameter	Average Weight (Expert Rating)	Normalized Weight	Final Index
DIFN	0.35	0.70	DIFN <sup>0.7</sup>
Н	0.15	0.30	$H^{0.3}$

**Table 2.** Parameter weights and index conversion determined by the expert scoring method.

Among these components, due to its diminishing marginal effect, Cw adopts a logarithmic function form and does not participate in exponential weighting. However, experts also recommend setting its coefficient at 0.5.

0.90

0.10

 $LAI^{0.9}$ 

ln(1 + 0.5Cw)

## 2.1.3. Variable Control

0.45

0.05

LAI

Cw

As the CSI serves as the primary variable considered in this study, we designed five canopy environment classes in the experiment, classified according to CSI values as follows (Table 3):

Forests **2025**, *16*, 1576 8 of 25

**Table 3.** Canopy environmental grade.

CSI_Level	Rank
level $\leq 0.15$	5
$0.15 \le \text{level} < 0.20$	4
$0.20 \le level < 0.25$	3
$0.25 \le level < 0.30$	2
level > 0.30	1

#### 2.2. Recruitment of Subjects

Through stratified sampling from the Guangdong University of Technology student database, 42 healthy college student volunteers were ultimately recruited (17 males and 25 females, aged 18–25 years, with a mean age of  $22.3 \pm 1.2$  years). Among them, 32 participants came from majors related to landscape architecture, and 10 participants came from other fields. Due to the limitations of the experimental site, this experiment is currently recruiting only students. All participants passed Ishihara color blindness tests and Snellen visual acuity screening (corrected vision  $\geq$  1.0), signed informed consent forms prior to the experiment, and were screened for anxiety tendencies using the GAD-7 scale (score < 5). To control circadian rhythm effects, the experiment was scheduled during two time slots on weekdays: 9:00–12:00 and 14:00–17:00, with participants randomly assigned to different time slot groups. Participants were prohibited from consuming caffeine or alcoholic beverages 24 h before the experiment and were required to maintain at least 7 h of sleep the preceding night. Upon arriving at the laboratory, participants sat quietly for 15 min to acclimate to the environment. During this time, the experimenter explained the procedures and conducted equipment-wearing adaptation training. All participants in the experiment filled out informed consent forms.

#### 2.3. Experimental Setup

The experiment was conducted in the Eye Movement and Physiological Laboratory at Guangdong University of Technology, equipped with eye trackers and physiological monitoring devices to create an immersive experimental environment. Sessions were held on weekdays during two time slots (9:00–12:00 and 14:00–17:00), with illumination intensity maintained at constant levels and background noise controlled below 35 dB(A). Participants sat in Ergohuman ergonomic chairs, with their heads stabilized in the eye tracker calibration position by adjustable headrests, maintaining a 2.3-m viewing distance from the center of the screen (corresponding to a 58° retinal angle). ErgolabLAB 3.0 software was used to record participants' physiological data and eye movement metrics throughout the experiment.

#### 2.4. Experimental Procedure

## 2.4.1. Equipment Configuration and Calibration

The experiment employed a multimodal synchronous acquisition system. Physiological signals were collected using an EXG acquisition device to record HRV, with an ECG signal sampling frequency of 0.05–200 Hz. Eye movements were captured via an HTC Vive Pro 2 VR head-mounted eye tracker with a sampling frequency of 50 Hz. After the devices were fitted, a 9-point eye movement calibration procedure was executed to ensure a gaze point error of less than  $0.6^{\circ}$  (calibration standard based on the eye tracker manufacturer's technical specifications).

#### 2.4.2. Experimental Stage Design

A Latin square design was used to balance scene order effects. Each experimental session comprised four standardized phases (Figure 5). First, emotional baseline calibration: a 10-s display of a neutral landscape image (sourced from the ISO 12901-2 certified NSN-2017 image database) to establish physiological response baselines. Second, street scene exposure: sequential display of 3 panoramic images of the target street, each presented for 30 s, with transitions using 5-s neutral gray screens (RGB 128, 128, 128). Finally, synchronous data acquisition: recording the following data for five street scenes: eye movement trajectory heatmaps, fixation duration, pupil diameter changes, and HRV time-frequency domain metrics (e.g., SDNN, RMSSD, LF/HF).

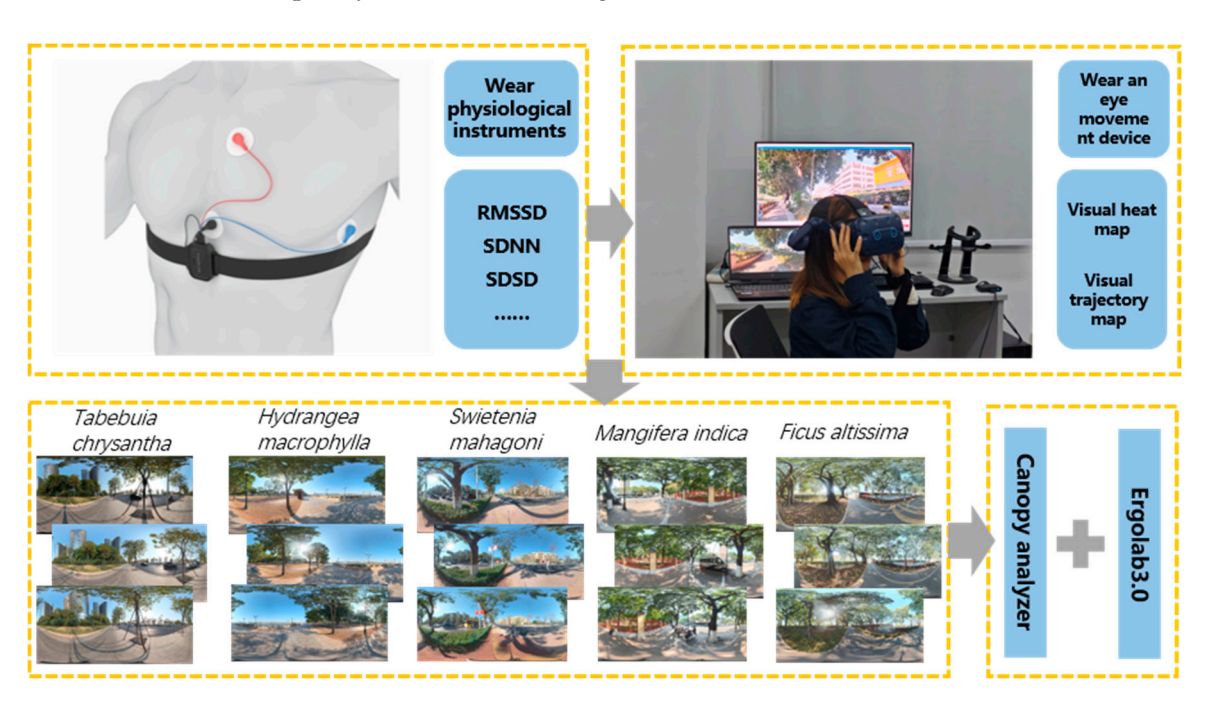


Figure 5. Experimental flowchart.

#### 2.4.3. Control Measures and Intermittent Design

To ensure data reliability, the following controls were implemented. First, inter-scene rest: After each set of scene tests, a 1-min rest period with eyes closed was provided, accompanied by full-spectrum white noise (20–20,000 Hz) to block environmental interference. Second, time control: The total duration of a single experiment was 30  $\pm$  2 min, and the transition screens were strictly timed with an error of less than 0.1 s.

### 3. Data Processing

#### 3.1. Canopy Image Processing

Hemispherical canopy images were acquired using a Sony ILCE-ZV10 camera equipped with a fisheye lens, with 10 standard trees selected from each street for photography, for a total of 50 images. The raw images underwent standardized processing through DJ-GC02 analysis software. The preprocessing phase entailed the following steps: first, geometric distortion correction was performed to eliminate lens edge deformation; second, illumination homogenization was implemented to reduce ambient light interference. Subsequently, canopy gap analysis was conducted. An adaptive threshold algorithm was applied to segment sky pixels (gaps) from leaf/branch pixels (non-gaps). The gap fraction distribution was statistically analyzed for each zenith angle (0° $\sim$ 90° at 10° intervals) and

azimuth angle  $(0^{\circ} \sim 360^{\circ})$  (Figure 6). Subsequent to the execution of the aforementioned steps, the LAI and DIFN parameters for each tree species were exported.

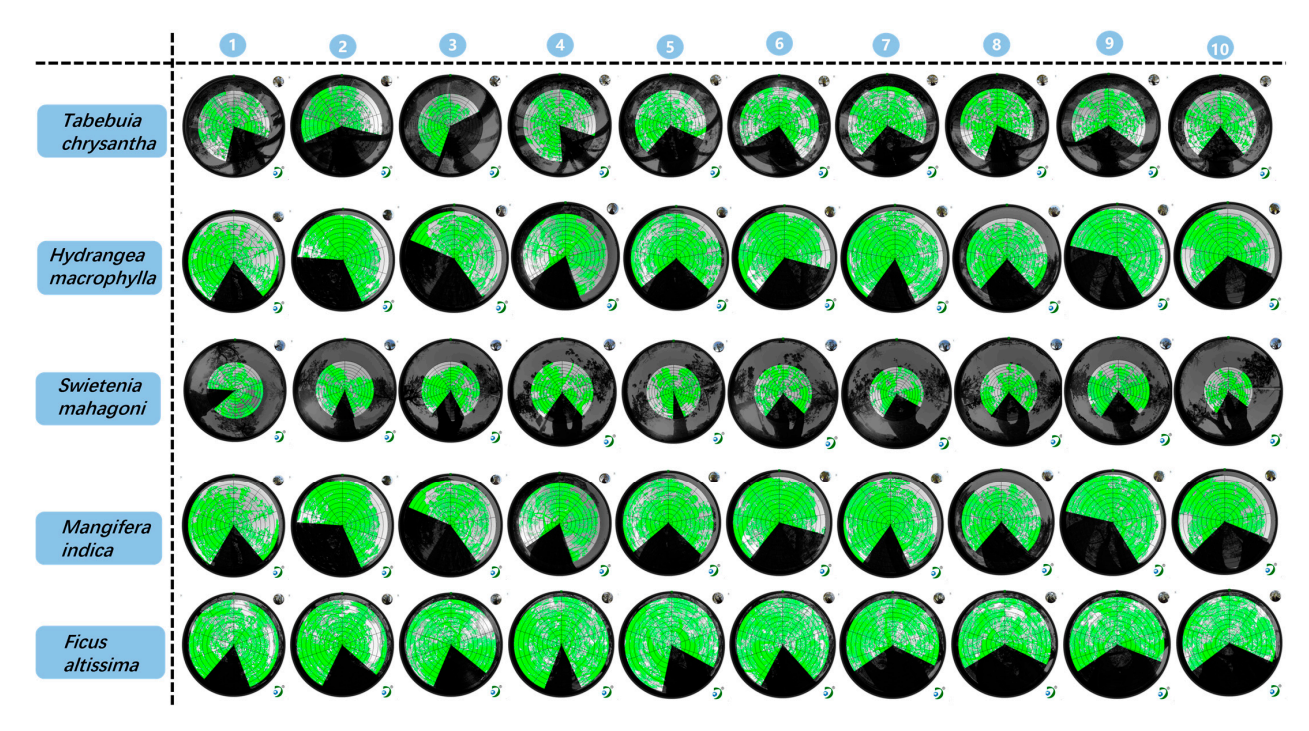


Figure 6. Distribution map of the canopy layer of street trees.

#### 3.2. Mental Stress Indicators Based on HRV Analysis

HRV is a highly valuable metric in the field of stress assessment. According to the HRV standards issued by the European Society of Cardiology and the American Heart Association in 1996, the calculation of HRV through ECG (electrocardiogram) and PPG (photoplethysmography) enables the evaluation of stress by means of analyzing the sympathetic and parasympathetic nervous systems. This approach has demonstrated excellent assessment outcomes in the field of stress exposure measurement [14].

The human body's stress response to psychological pressure primarily relies on regulation by the sympathetic and parasympathetic nervous systems. The excitation of the sympathetic nervous system has been demonstrated to promote the contraction of the myocardium and peripheral blood vessels, thereby adjusting the cardiovascular system to adapt to stress states. Conversely, when the body is in a relaxed state, the parasympathetic nervous system becomes relatively excited, enabling the cardiovascular system to adapt to relaxation, resulting in corresponding changes in HRV [15-17]. The low-frequency and high-frequency components of the HRV power spectrum have been demonstrated to reflect the activity of the sympathetic and parasympathetic nervous systems, respectively, and the low-frequency to high-frequency energy ratio can serve as an indicator of the balance between the two systems [18]. In situations involving stress, the low-frequency component of HRV has been observed to undergo a relative increase during relaxation; parasympathetic nervous system excitation leads to a relative increase in the high-frequency component of HRV. Therefore, in this experiment, we assessed the mental stress state of subjects by comparing various HRV analysis metrics. Physiological data from all subjects were imported into ErgoLAB 3.0 software for analysis, with some preprocessing required prior to analysis.

#### 3.2.1. HRV Signal Preprocessing

The first step is Wavelet Denoise. Through the wavelet transform, the wavelet coefficients generated by the signal contain important information about the HRV signal.

Forests 2025, 16, 1576 11 of 25

After wavelet decomposition, the wavelet coefficients of the signal are larger than those of the noise, while the wavelet coefficients of the noise are smaller than those of the signal. Selecting an appropriate threshold allows us to consider wavelet coefficients greater than the threshold as valid signals. Those smaller than the threshold are deemed to be generated by noise and are set to zero in order to achieve denoising.

The second step is High/Low Pass. The frequency range of ECG signals is 0.01–200 Hz, while the frequency range of pulse signals is 0.1–40 Hz. High-pass and low-pass filters remove noise signals while retaining valid data frequency bands.

The third step is Band Pass. It is primarily used to remove power frequency interference in the environment. The frequency is generally 50 Hz or 60 Hz, mainly manifested as sine waves or other signals superimposed on sine waves during signal measurement.

The fourth step is Ectopic Interval Detection. This method identifies intervals that deviate from the previous interval by a user-defined percentage (typically 20%) as abnormal intervals. Another method is the median filter, which acts as an impulse suppressor with a threshold that delineates ectopic intervals. Ectopic detection is performed based on a user-defined window length. Equation (2)

$$D(n) = \frac{|x(n) - med(x)|}{1.483 \ med(x(n) - med(x))}$$
(2)

if D (n)  $\geq \tau$ , then not ectopic; else ectopic

Here, D (n): the standardized absolute deviation of the n-th data point. A larger D (n) value indicates a higher likelihood of the point being anomalous. x (n): the original value of the n-th point in the input data sequence. med (x): the median of the entire data sequence x. |x|(n) - med(x)|: the absolute deviation between the current data point and the median of the entire sequence, reflecting the absolute distance of the point relative to the data center. med|x|(n) - med(x)|: the median of the absolute deviations of all data points from the median, representing the typical degree of data point deviation. 1.483: a scaling factor used to convert the median of absolute deviations into a robust estimate of the standard deviation.  $\tau$  (tau): the decision threshold, set by the user based on specific application scenarios and sensitivity requirements. If D (n)  $\geq \tau$ , the point is determined not to be an ectopic point; if D (n)  $< \tau$ , it is identified as an ectopic point.

The final step is Ectopic Interval Correction. The mean method replaces the ectopic interval with the mean of w adjacent IBI intervals centered on the ectopic interval, using Equation (3). Similarly, the median method replaces the ectopic interval with the median of w adjacent IBI intervals. Finally, it substitutes the ectopic interval using a cubic spline function with Equation (4).

"
$$ibi'(n) = mean(ibi(n+m)), where |m| \le \frac{w-1}{2}$$
 (3)

"
$$ibi'(n) = med(ibi(n+m)), where |m| \le \frac{w-1}{2}$$
 (4)

#### 3.2.2. HRV Analysis

#### (1) IBI Extraction

In HRV analysis, the data sequence is a time series of beat intervals extracted from an electrocardiogram (ECG) or pulse signals. The temporal location of the beats is typically determined based on the R-wave, which exhibits the highest amplitude. Thus, the interval between consecutive heartbeats can be defined as the time difference between successive R-peaks (RR interval). RR intervals originating from normal sinus rhythm are sometimes termed NN (normal-to-normal) intervals, where the "NN" nomenclature replaces "IBI"

Forests 2025, 16, 1576 12 of 25

or "RR" to emphasize the exclusion of ectopic intervals from the IBI series. Most current studies use RR or NN intervals to represent the IBI series, assuming that ectopic intervals have been corrected. The IBI interval is calculated as:

$$IBI_n = R_{n+1} - R_n \tag{5}$$

## (2) Time Domain Analysis

Time-domain HRV analysis evaluates heart rate variability by calculating a series of statistical metrics derived from R-R intervals, revealing temporal patterns in the signal. Time-domain metrics primarily reflect the tonic activity of the sympathetic and parasympathetic nervous systems, further assessing the overall regulatory capacity of the autonomic nervous system. Common time-domain indices include SDNN: Standard deviation of NN intervals; RMSSD: Root mean square of successive differences between IBIs; and pNNx: Percentage of consecutive intervals differing by more than x milliseconds (typically pNN50 or pNN20).

The standard deviation of the SDNN RR interval is calculated using the following formula:

$$SDNN = \sqrt{\frac{1}{N} \sum_{i=1}^{N} \left( RR_i - \overline{RR} \right)^2}$$
 (6)

where N represents the total number of normal heartbeats,  $RR_i$  denotes the i-th RR interval, and  $\overline{RR}$  signifies the average value of the RR interval for the N-th heartbeat.

The following formula will calculate the standard deviation of the SDANN cardiac cycle mean value:

$$SDANN = \sqrt{\frac{1}{N} \sum_{i=1}^{N} \left( \overline{RR_i} - \overline{RR_x} \right)^2}$$
 (7)

where  $\overline{RR}_i$  refers to the mean value of RR intervals in the i-th segment of data, and  $\overline{RR}_x$  refers to the mean value of RR intervals in all segmented data.

RMSSD Root-mean-square formula for consecutive adjacent cardiac cycle values:

$$RMSSD = \sqrt{\frac{1}{N-1} \sum_{i=1}^{N-1} \left( RR_{(i+1)} - RR_i \right)^2}$$
 (8)

where N denotes the total number of normal heartbeats, and  $RR_{(i+1)}$  and  $RR_i$  represent the lengths of two adjacent cardiac cycles.

## (3) Frequency Domain Analysis

Heart rate fluctuations are often considered periodic and can be quantified by calculating the Power Spectral Density (PSD) of the IBI time series. PSD represents the spectral power density of the time series as a function of frequency, generating a heart rate power spectrum with frequency on the horizontal axis and energy on the vertical axis, thereby revealing the distribution of energy across different frequencies. The following figure is a frequency domain analysis diagram (Figure 7).

Frequency-domain HRV analysis typically relates to four spectral bands: ULF (0–0.0033 Hz), VLF (0.0033–0.04 Hz), LF (0.04–0.15 Hz), and HF (0.15–0.4 Hz). In this experiment, the LF/HF ratio is used as the key metric.

#### (4) Nonlinear Analysis

Due to the non-stationary and nonlinear nature of HRV, further analysis employs nonlinear methods, including Poincaré plots, which are scatter diagrams of consecutive intervals, and difference scatter plots, which visualize differences between successive intervals.

Forests 2025, 16, 1576 13 of 25

omain											
Interval	Power Percentage	Normalized Pow	er Peak		nit: ms²/Hz	X Unit	Hz		PSI	HF	L
0 -0.0033Hz	54.69ms <sup>2</sup> 2.16%	0	0.003Hz	_							1
0.0033-0.04Hz	905.84ms <sup>2</sup> 35.78%	0	0.025Hz	_							
0.04-0.15Hz	827.24ms <sup>2</sup> 32.68%	0	0.04Hz	1							
0.15 -0.4Hz	743.75ms <sup>2</sup> 29.38%	0.47	0.255Hz	0.00	0.05	0.10	0.15	0.20	0.25	0.30	
	Interval 0 -0.0033Hz 0.0033-0.04Hz 0.04-0.15Hz	Interval Power Power Percentage   0 -0.0033Hz 54.69ms² 2.16%   0.0033-0.04Hz 905.84ms² 35.78%   0.04-0.15Hz 827.24ms² 32.68%	Interval Power Power Percentage Normalized Power   0 -0.0033Hz 54.69ms² 2.16% 0   0.0033-0.04Hz 905.84ms² 35.78% 0   0.04-0.15Hz 827.24ms² 32.68% 0	Interval Power Power Percentage Normalized Power Peak   0 -0.0033Hz 54.69ms² 2.16% 0 0.003Hz   0.0033-0.04Hz 905.84ms² 35.78% 0 0.025Hz   0.04-0.15Hz 827.24ms² 32.68% 0 0.04Hz	Interval Power Power Percentage Normalized Power Peak   0 -0.0033Hz 54.69ms² 2.16% 0 0.003Hz   0.0033-0.04Hz 905.84ms² 35.78% 0 0.025Hz   0.04-0.15Hz 827.24ms² 32.68% 0 0.04Hz	Interval Power Power Percentage Normalized Power Peak   0 -0.0033Hz 54.69ms² 2.16% 0 0.003Hz   0.0033-0.04Hz 905.84ms² 35.78% 0 0.025Hz   0.04-0.15Hz 827.24ms² 32.68% 0 0.04Hz	Interval Power Power Percentage Normalized Power Peak   0 -0.0033Hz 54.69ms² 2.16% 0 0.003Hz   0.0033-0.04Hz 905.84ms² 35.78% 0 0.025Hz   0.04-0.15Hz 827.24ms² 32.68% 0 0.04Hz	Interval   Power   Power   Percentage   Normalized   Power   Peak	Interval   Power   Power   Percentage   Normalized   Power   Peak	Interval   Power   Power   Power   Power   Peak	Interval   Power   Power Percentage   Normalized Power   Peak

Figure 7. Frequency domain analysis of HRV.

Based on the premise that each IBI is influenced by its preceding IBI, Poincaré plots reveal correlations between consecutive values in the time series (Figure 8). SD1: Standard deviation along the ellipse's major axis, representing short-term variability. It primarily reflects parasympathetic activity—when SD1 decreases, parasympathetic activity diminishes, and sympathetic activity increases. SD2: Standard deviation along the ellipse's minor axis, representing long-term variability. It correlates more strongly with sympathetic activity than parasympathetic activity—when SD2 decreases, sympathetic activity intensifies.

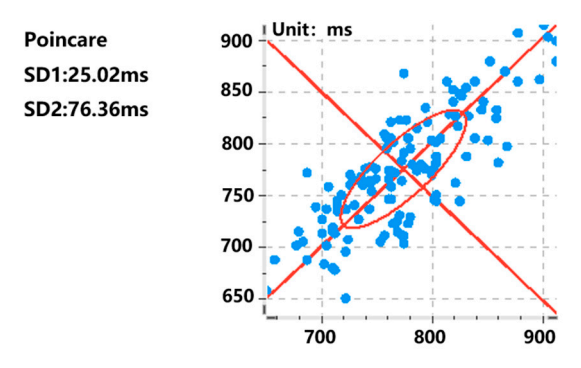


Figure 8. Bondegarre scatter plots.

A difference scatter plot is a graphical representation that utilizes the difference between three consecutive IBI points to obtain a coordinate point, illustrating the correlation between consecutive rate values in a time series (Figure 9). Key metrics include: A++: Points in the first quadrant indicate two successive increases in beat intervals (heart rate deceleration), representing parasympathetic activity. B--: Points in the third quadrant indicate two straight decreases in beat intervals (heart rate acceleration), representing sympathetic activity. Note: Axes are labeled in milliseconds (ms). The following table provides a detailed explanation of all HRV indicators (Table 4).

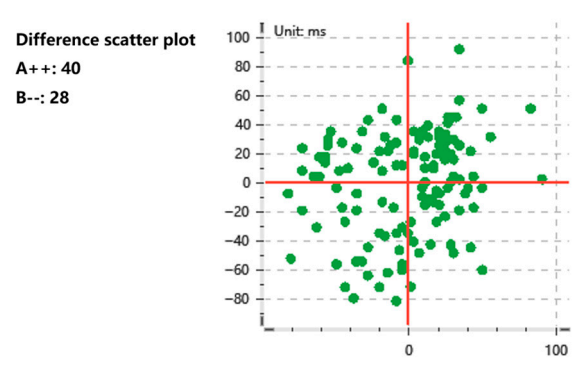


Figure 9. Difference scatter plots.

Table 4.	HRV	analyz	es various	indicators.

Index	Unit	Meaning
MeanIBI	ms	Mean value of all N-N intervals, or cardiac intervals, during the entire recording period.
MeanHR	Bpm	The average heart rate value of the ECG signal.
SDNN	ms	Standard deviation of all N-N intervals, or cardiac intervals, during the entire recording period.
RMSSD	ms	Mean value of differences between adjacent RR intervals.
SDSD	ms	Standard deviation of successive differences between adjacent RR intervals.
pNN50	%	Percentage of adjacent heartbeats with differences exceeding 50 ms relative to the total number of heartbeats.
pNN20	%	Percentage of adjacent heartbeats with differences exceeding 20 ms relative to the total number of heartbeats.
LF/HF		Ratio of low-frequency to high-frequency band power.
SD1	ms	Vertical deviation of cardiac intervals in Poincaré plots.
SD2	ms	Horizontal deviation of cardiac intervals in Poincaré plots.
A++		Number of points in the first quadrant of the difference scatter plot.
B		Number of points in the third quadrant of the difference scatter plot.

#### 3.2.3. HRV Data Processing

HRV data collected from 42 subjects during the five-street experiments were imported into SPSS 22 for processing. Due to excessive deviations in the experimental results of two subjects, their data were excluded. For the remaining 40 subjects, missing values were addressed using interpolation methods, and outliers were treated via Z-score standardization.

#### (1) Interpolation Method

Linear interpolation assumes that data varies linearly near the missing point. The linear interpolation function is:

$$x_i = \frac{x_{i-1} + x_{i+1}}{2} \tag{9}$$

#### (2) Z-Score Method

Outliers are identified via the Z-Score, defined as:

$$z = \frac{x_i - \mu}{\sigma} \tag{10}$$

#### 3.3. Attention-Related Metrics

## 3.3.1. Application of Eye-Tracking Experiment

Vision serves as the primary mode of acquiring information, capturing significantly more data than the other senses. It is a critical pathway through which humans perceive the external environment. Visual behavior is a fundamental mode of perception and imagination [19]. The use of eye-tracking technology to study how individuals' process information has become a central focus in psychological research, with rapidly expanding applications across disciplines. Eye movements comprise three basic patterns: fixation, saccades, and pursuit movements, which often intertwine to reveal selective attention during information perception [20]. Currently, eye-tracking technology is increasingly applied in fields such as architectural and spatial perception, landscape experience and design, wayfinding experiments, and urban spatial cognition [21]. For example, Sun Cheng et al. [22] investigated perceptual patterns of visual saliency for landmarks during indoor wayfinding; Wang et al. [23], combining dynamic VR with eye-tracking, found that natural elements like "sky," "trees," and "water features" in campus environments positively correlated with psychological restoration dimensions of "being away" and "fascination," whereas artificial elements like "building corridors" negatively impacted restorative effects, supporting the principle of prioritizing nature in campus design; Chen Yiyan et al. [24], using head-mounted eye-trackers to analyze Shanghai's Nanjing Road Pedestrian Street, discovered that "information density" (the ratio of fixation proportion to screen area coverage) was highest for exterior signage, building entrances, and brand

Forests 2025, 16, 1576 15 of 25

logos, significantly influencing pedestrian visual experiences. Systematic design of such elements can shape distinctive streetscape characteristics.

#### 3.3.2. Eye-Tracking Data Processing

Eye-tracking data from 40 subjects were processed using Ergolab 3.0 software to generate visual heatmaps and gaze trajectory maps. Simultaneously, the AOI Tool module was utilized for quantitative analysis of Areas of Interest (AOI) in the images. Given the study's focus on the impact of canopies on human perception, AOIs were specifically delineated for canopy regions in the research images, resulting in the identification of canopy AOIs (Figure 10). For each image, the First Fixation Duration (FHD) (unit: milliseconds) and the Duration Proportion of Fixations (DPF) within the canopy AOI were statistically analyzed. The calculation formula for DPF is defined as the percentage of total fixation time within the canopy AOI relative to the total fixation time across the entire scene (DPF =  $\Sigma$  single fixation duration within AOI/total fixation duration of full scene  $\times$  100%). First Fixation Duration reflects the attractiveness of the stimulus to subjects, while the Duration Proportion of Fixations indicates the strength of attention capture by a specific AOI.



Figure 10. The canopy interest areas of the five groups of streets.

## 4. Results

#### 4.1. Quantitative Characteristics of Canopy Morphological Parameters

The processed parameters of the street trees across five streets—H, Cw, LAI, DIFN—were substituted into the CSI formula, yielding the results shown in Table 5. The calculated CSI values for each tree fall within the predefined CSI\_level interval ranges.

Table 5	The CSI	distribution	of five	street trees.
Table 5.	The Cor	aistribution	or nive	street trees.

Tree	CSI Mean	CSI_Level	Rank
Ficus altissima	0.121	level $\leq 0.15$	5
Mangifera indica	0.177	$0.15 \le level < 0.20$	4
Swietenia mahagoni	0.222	$0.20 \le level < 0.25$	3
Hydrangea macrophylla	0.275	$0.25 \le level < 0.30$	2
Tabebuia chrysantha	0.321	level > 0.30	1

In the Quantitative Analysis of Canopy Morphological Parameters for Street Trees, significant differences were observed in the structural characteristics of the five tree species. The five tree species exhibited significant differences in morphological parameters due to their canopy structural characteristics. Their CSI values demonstrated a gradient classification, with Golden Trumpet Tree (*Tabebuia chrysantha*) showing the highest average

Forests 2025, 16, 1576 16 of 25

CSI (0.321), while *Ficus altissima* had the lowest average CSI (0.121). These species were categorized into five levels (1–5) according to the initial classification. The following figure shows the canopy distribution of five roadside trees (Figure 11). Comparative averages of other parameters are as follows:

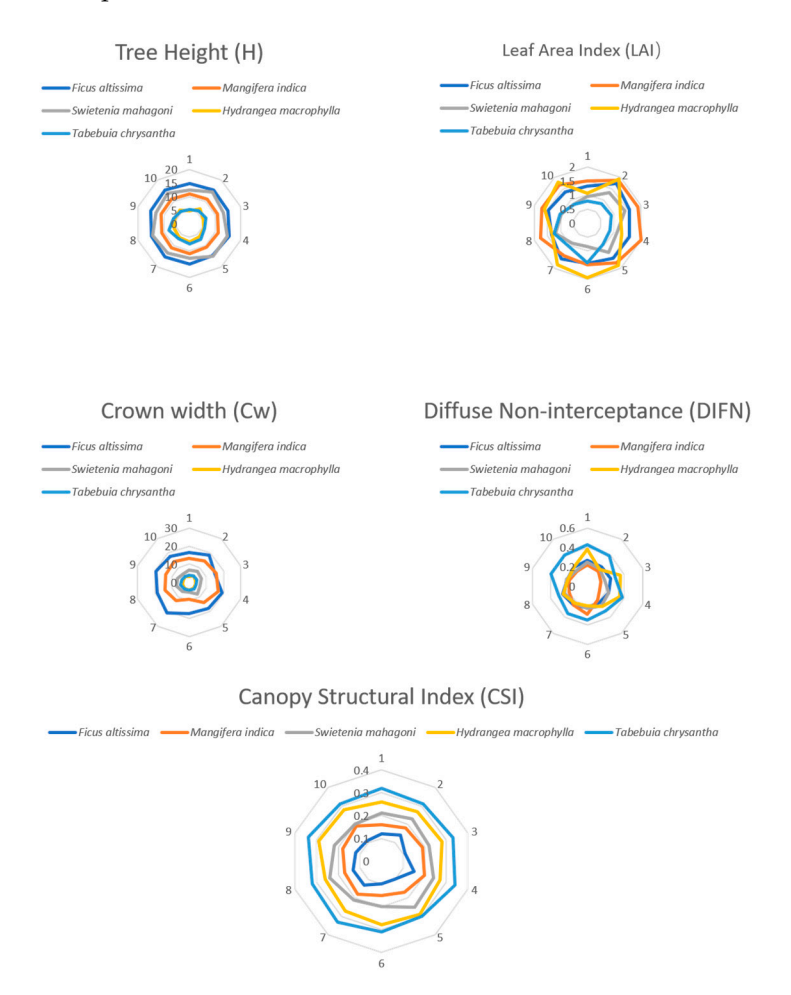


**Figure 11.** The canopy distribution of five street trees.

H: Ficus altissima (15.08 m) > Swietenia mahagoni (13.74 m) > Mangifera indica (11.08 m) > Hydrangea macrophylla (6.01 m) > Tabebuia chrysantha (6.49 m).

Cw: Ficus altissima (18.10 m) > Mangifera indica (13.82 m) > Tabebuia chrysantha (4.27 m) > Swietenia mahagoni (6.78 m) > Hydrangea macrophylla (3.93 m).

LAI: Mangifera indica  $(1.71 \text{ m}^{-1}) > Hydrangea macrophylla <math>(1.59 \text{ m}^{-1}) > Ficus \ altissima (1.49 \text{ m}^{-1}) > Swietenia mahagoni <math>(1.08 \text{ m}^{-1}) > Tabebuia \ chrysantha (0.98 \text{ m}^{-1})$ .

DIFN: Tabebuia chrysantha (0.36) > Hydrangea macrophylla (0.27) > Ficus altissima (0.24) > Swietenia mahagoni (0.23) > Mangifera indica (0.20).

#### 4.2. Mental Stress Detection Based on HRV Analysis

#### 4.2.1. Based on HRV Analysis

An in-depth analysis of 12 HRV metrics collected from 40 healthy subjects after intervention trials was conducted. Paired-sample t-tests were used to construct 95% confidence intervals, and strict statistical criteria were applied to identify HRV features with significant intergroup differences across five streets with varying CSI levels. This provides quantitative evidence for objectively assessing environmental stress levels. Data analysis revealed that the two-tailed p-values for SD1, SD2, A++, and B-- exceeded 0.05. Thus, they were excluded

based on significance criteria. The two-tailed *p*-values for the remaining eight metrics were all less than 0.05. The specific data are presented in Table 6.

Table	6	The	rocui	ا+ د	√f I	IRV

Index	CSI = 1	CSI = 2	CSI = 3	CSI = 4	CSI = 5
MeanIBI/ms	823.14	837.83	853.61	869.24	885.919
MeanHR/bpm	73.18	71.68	69.73	67.70	65.575
SDNN/ms	39.51	43.59	47.81	52.01	56.54425
RMSSD/ms	27.54	31.10	35.14	39.37	43.96075
SDSD/ms	27.51	31.06	35.11	39.33	43.92825
Pnn50/%	22.62	26.60	30.52	34.74	39.27125
Pnn20/%	62.67	65.70	68.84	72.16	75.9955
LF/HF	2.11	1.75	1.42	1.12	0.87325

Observing their mean values revealed that MeanIBI, SDNN, RMSSD, SDSD, Pnn50, and Pnn20 exhibited significant linear upward trends with increasing CSI levels, indicating significant positive correlations (Figure 12).

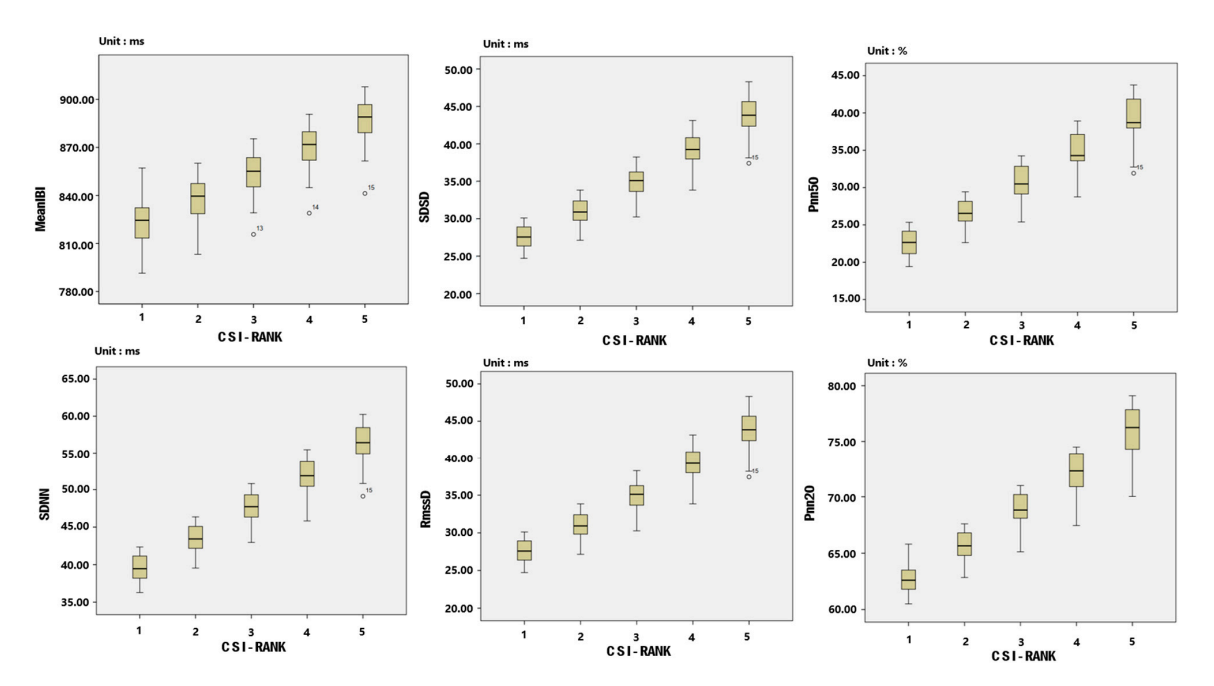


Figure 12. Box plot of HRV feature distribution (Part 1).

Conversely, the MeanHR and the LF/HF showed significant downward trends with higher CSI levels, demonstrating a significant negative correlation (Figure 13).

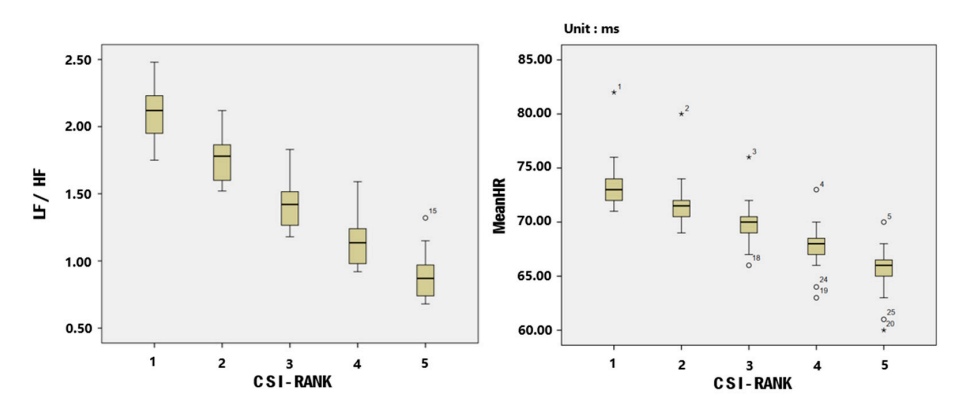


Figure 13. Box plot of HRV feature distribution (Part 2).

Forests 2025, 16, 1576 18 of 25

In line with the consensus of prior research, characteristic changes in HRV parameters during the transition from stress to relaxation include significantly increased time-domain metrics (e.g., SDNN, pNN50, and pNN20) and frequency-domain metrics (e.g., RMSSD and SDSD), alongside significantly decreased MeanHR and LF/HF ratios. These results demonstrate that, as CSI levels increase, HRV parameter shifts align closely with relaxation-state patterns, indicating that high-CSI environments effectively mitigate psychological stress by modulating autonomic nervous system activity.

#### 4.2.2. Distribution Status of HRV Indicators Under Different CSI Levels

Similarly, we separately analyzed the distribution of HRV metrics under different CSI levels while subjects were in their most relaxed states. Specifically, we examined the percentage of occurrences in which the following metrics reached their maximum values relative to total occurrences: MeanIBI, SDNN, RMSSD, SDSD, pNN50, and pNN20. We also examined the percentage of occurrences in which the following metrics reached their minimum values relative to total occurrences: MeanHR and LF/HF. The results are shown in Figure 14.

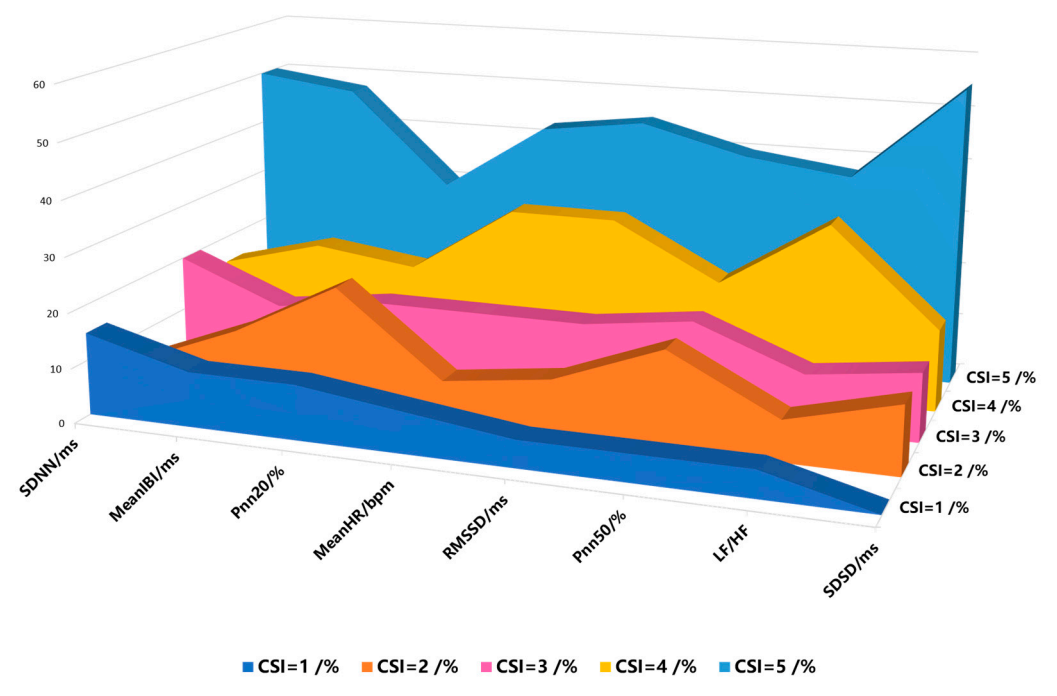


Figure 14. Distribution status of different indicators under different CSI levels in the most relaxed state.

From a holistic data analysis perspective, the frequency of multiple HRV metrics indicating optimal relaxation states among subjects peaked when the CSI level reached 5, a finding consistent with previously accumulated full-sample data. As CSI levels increased, the occurrence frequency of most HRV metrics corresponding to the most relaxed states showed an upward trend, though some metrics exhibited non-monotonic changes. For example, in the comparison between CSI levels 2 and 3, a higher proportion of subjects achieved the most relaxed state for the pNN20 metric at CSI level 2 than at level 3. This difference may be due to individual physiological variability among subjects.

Notably, not all subjects reached their optimal relaxation states at CSI level 5, a divergence closely linked to heterogeneity in individual environmental preferences. Significant differences in perceptual thresholds, adaptive capacities, and subjective preferences to environmental stimuli resulted in varied comfort parameters across individuals. However, this individual-level variability did not substantially impact the overall statistical significance

Forests 2025, 16, 1576 19 of 25

of the study, which robustly demonstrates the correlation between Canopy Structural Index levels and psychological stress mitigation.

## 4.3. Attention Detection Based on Eye-Tracking Data

First, the FHD and the DPF were visualized in the canopy ROI of each collected image (Figures 15 and 16). Second, visual heatmaps and trajectory maps were obtained for each photo at different canopy feature CSI levels by importing eye movement data from 40 subjects (Figures 17 and 18). Finally, the following results were obtained.

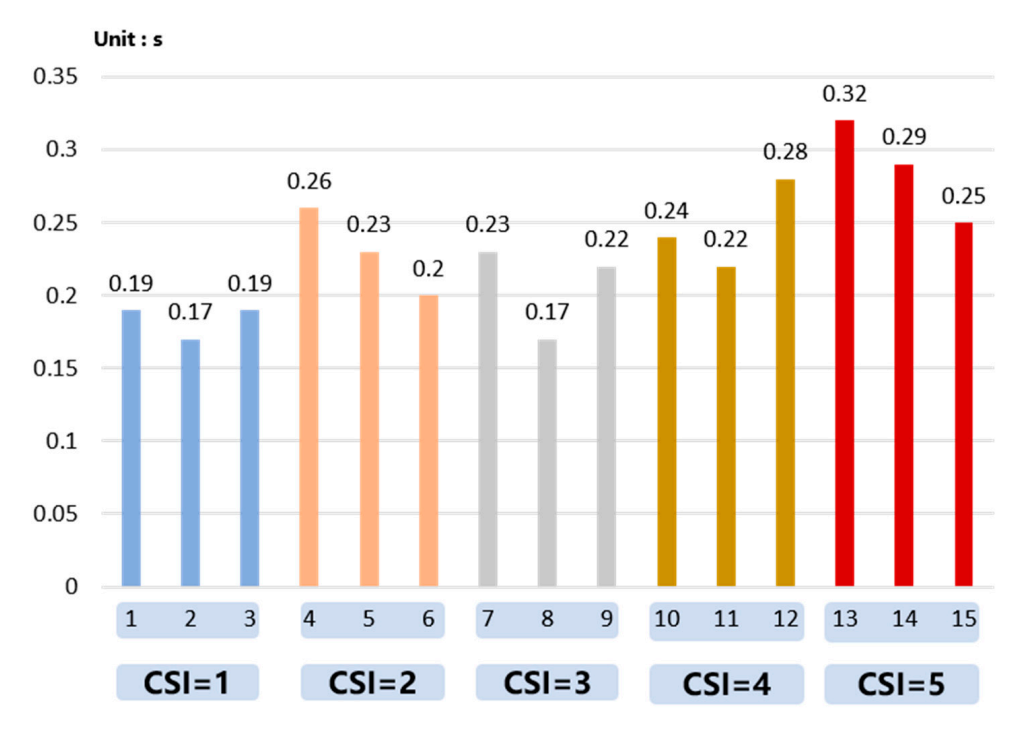


Figure 15. The mean result of FFD in the coronal region of interest.

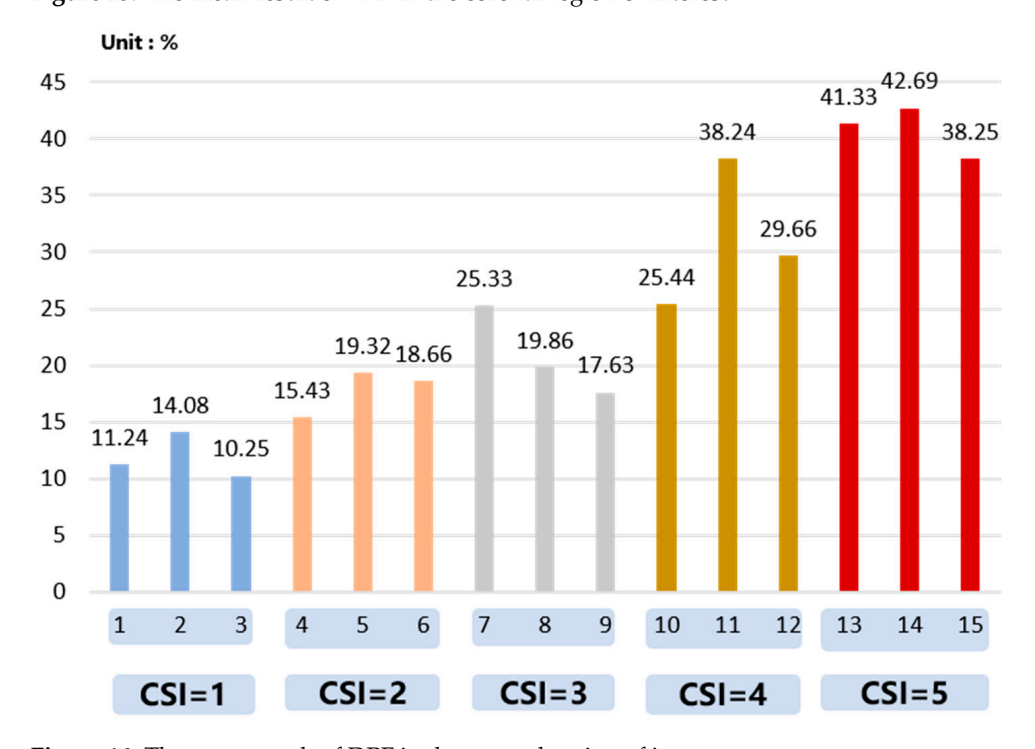


Figure 16. The mean result of DPF in the coronal region of interest.

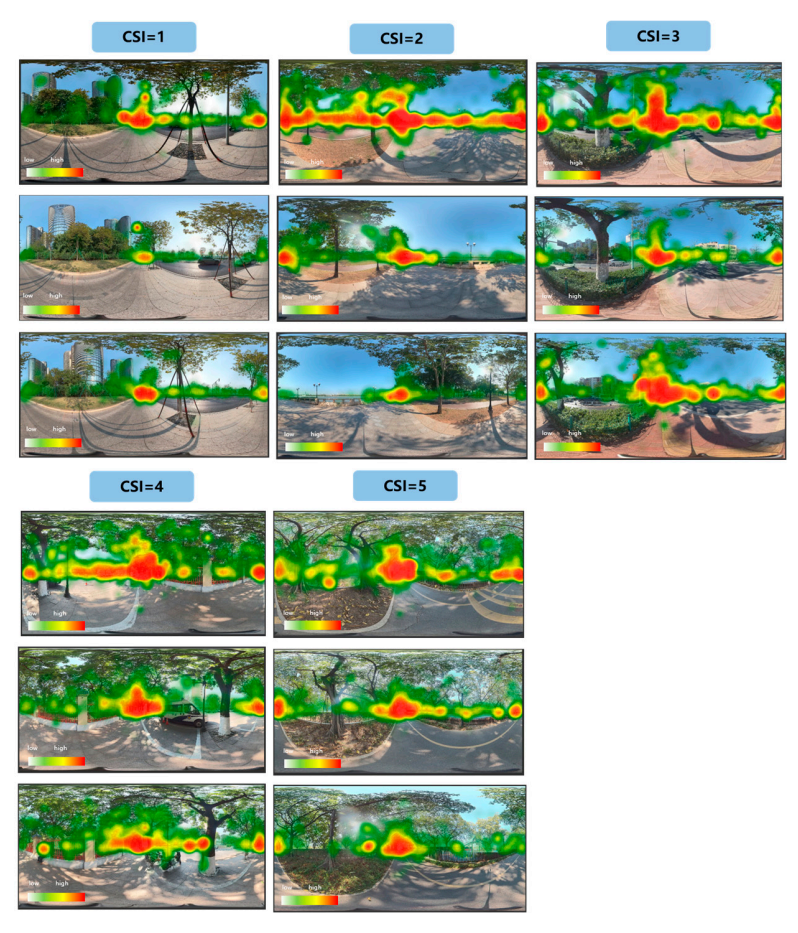


Figure 17. Visual heat map.



Figure 18. Visual trajectory map.

Forests 2025, 16, 1576 21 of 25

#### 4.3.1. Based on FFD Analysis

Analysis of the mean FFD for canopy AOI under different CSI levels revealed that subjects' first fixation time on canopies generally exhibited a consistent distribution pattern (Figure 15). Notably, when CSI levels reached 4 and 5, the mean FFD showed a slight upward trend. Further observation of scenes with CSI levels 5 and 6 indicated that these two streets had relatively high canopy density, which may influence subjects' attention allocation. The results demonstrate that there were no significant differences in the visual attractiveness of street tree canopies across the five experimental streets. This finding provides important evidence for investigating the impact of street tree canopies on human perception because it effectively excludes the influence of other potential confounding factors.

## 4.3.2. Based on DPF Analysis

In the analysis of the mean DPF, the study observed a significant increasing trend in the proportion of gaze time devoted to canopy regions as CSI levels rose (Figure 16). Comparative analysis of environmental characteristics across the five streets revealed a positive correlation between canopy density and fixation duration. Under CSI level 5 in particular, subjects' DPF for canopies approached 50%, demonstrating a pronounced visual attraction effect. Overall, when subjects' visual attention focused on canopy areas, their points of interest concentrated significantly within these regions, indicating that denser canopy structures exert stronger visual guidance.

#### 4.3.3. Based on Visual Heatmap Analysis

The study found that, based on visual heatmap analysis under varying CSI levels, subjects' gaze distributions across all five street scenes exhibited a distinct front-central clustering pattern. This pattern aligns closely with natural pedestrian visual behavior while walking. This indicates that subjects primarily focused on the path ahead while walking naturally. Further analysis revealed that visual attention to canopy regions intensified significantly with higher CSI levels. Specifically, heatmap values for canopy areas notably increased at CSI levels 4 and 5, demonstrating that greater canopy density effectively directs visual focus.

#### 4.3.4. Based on Trajectory Analysis Graph Analysis

In gaze trajectory plots, the initial fixation points of all subjects clustered in the front-central target area, which is consistent with prior findings. Notably, under lower CSI levels (1–3), subjects' gaze trajectories rarely involved canopy regions, whereas at higher CSI levels (4–5), the proportion of gaze trajectories distributed over canopies increased significantly. Integrated heatmap and trajectory data indicate a positive correlation between subjects' visual preferences and CSI levels, with higher CSI levels corresponding to stronger visual attention concentration on canopy regions.

#### 5. Discussion

This study, set in the context of high-density, subtropical cities, innovatively constructed a comprehensive CSI and systematically revealed the profound effects of street tree canopy structures on pedestrians' psychophysiological responses. This was achieved by integrating HRV and eye-tracking technologies. The results not only quantified the physiological relaxation effects induced by different canopy morphologies but also uncovered the critical role of visual attention in this process. This discussion will address multiple aspects, including the innovativeness of the CSI metric, the mechanisms underlying physiological relaxation effects, the mediating role of visual attention, and the theoretical contributions and practical implications of this study.

Forests 2025, 16, 1576 22 of 25

## 5.1. Construction and Innovative Value of the Comprehensive Canopy Structural Index (CSI)

One of the core innovations of this study is the proposal of the Comprehensive CSI. In current research, scholars often use single-dimensional metrics such as LAI [25], canopy coverage, or simple morphological parameters (e.g., tree height, crown width) [26] to evaluate the ecological benefits of urban greening. The CSI constructed in this study integrates four key variables, H, Cw, DIFN, and LAI, to achieve a comprehensive quantification of both the physical form and optical properties of the canopy.

# 5.2. Quantitative Verification and Deepening of the Physiological Relaxation Effects of Street Tree Canopies

In this study, HRV analysis revealed that as CSI levels increased, metrics indicative of parasympathetic nervous activity (SDNN and RMSSD) significantly rose (by 15%-43%), while the LF/HF ratio, which reflects sympathetic and parasympathetic nervous systems, decreased significantly (by 31%). This finding is highly consistent with extensive literature on the role of natural environments in promoting physical and mental restoration. For example, multiple studies have confirmed that whether walking in a forest or merely viewing forest imagery, both can effectively enhance parasympathetic nervous system activity, reduce heart rate, and thereby facilitate physiological relaxation [27]. The contribution of this study lies in being the first to precisely miniaturize and validate these findings—originally framed within the macro "nature-urban" dichotomy—onto the specific element of "street tree canopy structure" within an urban context. In high-density subtropical cities, previous research has predominantly focused on the physical cooling and shading functions of street trees, namely their role in mitigating the urban heat island effect and enhancing pedestrian thermal comfort [28]. The title of this study, "Beyond Shade Provision," aptly highlights its core breakthrough. It demonstrates that street trees are valuable not only for providing shade but also for their visual morphology, which directly influences the human autonomic nervous system. This finding significantly enriches our understanding of the health benefits of urban green infrastructure, particularly in subtropical regions, emphasizing that while pursuing thermal comfort, the potential gains of canopy structures for psychophysiological health should not be overlooked.

## 5.3. The Central Role of Visual Attention Mechanisms in Human-Tree Environment Interactions

If HRV data answers the question of "whether canopy structure affects physiological state," then eye-tracking data further explains "how it affects." Although the potential of eye-tracking technology in environmental psychology has been recognized in existing literature [29], its direct application to investigate the linkage between visual perception of urban street tree canopies and physiological responses remains rare [30]. According to Attention Restoration Theory (ART), fascinating natural environments can help individuals recover from directed attention fatigue. The high-CSI-level canopies in this study, with their complex structures, fractal characteristics, and dynamic light-shadow variations, represent a typical "soft fascination" stimulus. Pedestrians shift their visual resources from monotonous, stressful urban artificial environments (e.g., building facades, traffic signs) and immerse themselves in prolonged "involuntary" observation of the canopy. This process itself may reduce stress and restore cognitive resources, ultimately manifesting as the enhanced parasympathetic activity indicated by HRV metrics. In addition, this study also found that pedestrians tend to focus their attention on the front central region when walking. Therefore, further design of street trees in cities can be targeted at this aspect to alter the impact on the visual experiences of pedestrians'. The canopy is not the only factor affecting comfort and aesthetics. However, the canopy structure likely plays a dominant role in first impressions and rapid visual perception. This aligns well with Forests 2025, 16, 1576 23 of 25

eye-tracking methodology, which is designed to capture immediate attentional responses. Future research will incorporate a more diverse set of characteristics for analysis.

#### 6. Conclusions

The following conclusions were drawn through quantitative analysis:

- (1) HRV analysis revealed significant differential effects of CSI levels on subjects' autonomic regulation. Intra-individual comparisons showed that as CSI levels increased, HRV metrics (e.g., SDNN and RMSSD) exhibited significant upward trends, while metrics such as MeanHR declined, indicating a physiological relaxation state dominated by parasympathetic nervous system activity.
- (2) Eye-tracking data demonstrated a strong correlation between CSI levels and patterns of visual attention allocation. Higher CSI levels significantly concentrated visual attention toward canopy regions.
- (3) Synthetically, when the CSI was below 0.15, most subjects achieved optimal psychological perception and visual preference for canopies. Thus, the selection and pruning of street trees should prioritize those with CSI values at or below a threshold of 0.15.

This study has several limitations.

- (1) The sample size of 40 participants is relatively limited (n = 40). Future research should expand the sample size and include more diverse populations (e.g., different ages, genders, cultural backgrounds, and occupations) to test the universality of the findings.
- (2) This study analyzed CSI as a comprehensive index and failed to analyze the independent contributions or interactive effects of individual factors such as H, Cw, LAI, and DIFN. Future experimental designs can use factor analysis to systematically deconstruct the unique impact weights of each component of CSI on psychological and physiological responses, which will make design recommendations more precise.
- (3) This study relied on objective physiological and behavioral data and lacked supplementary subjective semantic data. Future research should combine questionnaires, semantic differential methods, or interviews to collect pedestrians' subjective evaluations of canopies at different CSI levels (e.g., aesthetic appeal, sense of safety, feeling of relaxation, and preference). Then, researchers should analyze the consistency and differences between subjective perceptions and objective physiological responses. This would create a more comprehensive and holistic evaluation system.
- (4) The findings of this study are based on a subtropical urban context, and caution is needed when generalizing the conclusions to other climatic zones, such as temperate, cold, or arid regions. Because the needs and perceptual preferences of residents in different climatic regions regarding vegetation may vary, future comparative studies across climatic zones are highly valuable.

**Author Contributions:** Conceptualization, J.W. and Y.M.; methodology, J.W. and Y.M.; software, J.W. and J.H.; validation, J.W.; formal analysis, Y.M.; resources, J.W. and J.H.; data-curation, J.W. and J.H.; writing-original-draft-preparation, J.W. and Y.M.; writing-review. and editing, Y.M.; visualization, J.W. and J.H.; supervision, and Y.M.; project administration, Y.M.; funding acquisition, Y.M. All authors have read and agreed to the published version of the manuscript.

**Funding:** This research was funded by the Basic and Applied Basic Research Foundation of Guangdong Province in 2023, grant number 2023A1515011450 and The APC was funded by the Basic and Applied Basic Research Foundation of Guangdong Province in 2023.

**Data Availability Statement:** Data are available on request to the authors.

Conflicts of Interest: The authors declare no conflicts of interest.

Forests **2025**, 16, 1576 24 of 25

## **Abbreviations**

The following abbreviations are used in this manuscript:

CSI Canopy Structural Index

Cw crown width

DIFN diffuse non-interceptance

ECG electrocardiogram

H tree height

HRV heart rate variability LAI leaf area index

SNS sympathetic nervous system

### References

1. Nowak, D.J.; Dwyer, J.F. Understanding the Benefits and Costs of Urban Forest Ecosystems. In *Urban and Community Forestry in the Northeast*; Kuser, J.E., Ed.; Springer: Dordrecht, The Netherlands, 2007; pp. 25–46.

- 2. Xiong, J.; Qi, H.; Wang, Q.; Wang, S.; Zuo, W.; Sun, Y. Assessment of ecological benefit of street trees in urban community based on i-Tree model. *J. Nanjing For. Univ. Nat. Sci. Ed.* **2019**, *43*, 128–136.
- 3. Cai, Y.; Li, C.; Ye, L.; Xiao, L.; Gao, X.; Mo, L.; Du, H.; Zhou, Y.; Zhou, G. Effect of the roadside tree canopy structure and the surrounding on the daytime urban air temperature in summer. *Agric. For. Meteorol.* **2022**, *316*, 108850. [CrossRef]
- 4. Kaplan, R.; Kaplan, S. The Experience of Nature: A Psychological Perspective; Cambridge University Press: Cambridge, UK, 1989.
- 5. Wang, B.-B.; Cao, S.-Z.; Zhao, X.-G.; Huang, N.; Duan, X.-L.; Chen, Y.-T.; Jiang, Y.; Wang, L.-M. Investigation of soil contact time-related activity pattern of chinese adults. *J. Environ. Health* **2014**, *31*, 971–974. [CrossRef]
- 6. Fan, J.; Tang, H.; Ye, Y. Multi-dimensional evaluation and guidance for quality pedestrian street space: An analysis of multi-sourced urban data. *Planners* **2019**, *35*, 5–11.
- 7. Han, J.; Lee, S. Resident's Satisfaction in Street Landscape Using the Immersive Virtual Environment-Based Eye-Tracking Technique and Deep Learning Model. *Int. Arch. Photogramm. Remote Sens. Spat. Inf. Sci.* 2022, XLVIII-4/W4-2022, 45–52. [CrossRef]
- 8. Shao, Y.; Zhang, Z.; Jin, T. Research on the Perception and Influence Mechanism of Landscape Audio-visual Environment Elements in Residential Areas Along Urban Expressways: Take Shanghai as an Example. *Chin. Landsc. Archit.* 2025, 41, 55–62. [CrossRef]
- 9. Li, X.; Wu, D.; Li, L.; Wang, X. Research on visual perception evaluation of urban riverside greenway landscape based on deep learning. *J. Beijing For. Univ.* **2021**, *43*, 93–104.
- 10. Li, C.; Du, C.; Ge, S.; Tong, T. An eye-tracking study on visual perception of vegetation permeability in virtual reality forest exposure. *Front. Public Health* **2023**, *11*, 1089423. [CrossRef]
- 11. Zhu, H.P.; Kong, Y.H.; Ohno, R. Research Progress on Ambient Visual Information Analysis and Perception Measurement Methods for Motion Vision. *Landsc. Archit.* **2025**, *32*, 12–21.
- 12. Gong, C.; Yang, X.Y. Research on embodied perception of stairway space in mountain city parks based on multimodal data. *New Archit.* 2024, 4–10. [CrossRef]
- 13. Bratman, G.N.; Anderson, C.B.; Berman, M.G.; Cochran, B.; de Vries, S.; Flanders, J.; Folke, C.; Frumkin, H.; Gross, J.J.; Hartig, T.; et al. Nature and mental health: An ecosystem service perspective. *Sci. Adv.* **2019**, *5*, eaax0903. [CrossRef]
- 14. Task Force of the European Society of Cardiology and the North American Society of Pacing and Electrophysiology. Heart rate variability: Standards of measurement, physiological interpretation and clinical use. *Circulation* **1996**, *93*, 1043–1065.
- 15. Gaggioli, A.; Cipresso, P.; Serino, S.; Campanaro, D.M.; Pallavicini, F.; Wiederhold, B.K.; Riva, G. Positive technology: A free mobile platform for the self-management of psychological stress. *Stud. Health Technol. Inform.* **2014**, 199, 25–29.
- 16. Saalfield, J.; Spear, L. Developmental differences in the effects of alcohol and stress on heart rate variability. *Physiol. Behav.* **2014**, 135, 72–80. [CrossRef]
- 17. Choi, J.; Ahmed, B.; Gutierrez-Osuna, R. Development and Evaluation of an Ambulatory Stress Monitor Based on Wearable Sensors. *IEEE Trans. Inf. Technol. Biomed.* **2012**, *16*, 279–286. [CrossRef] [PubMed]
- 18. Lingqin, K.; Fei, C.; Yuejin, Z.; Liquan, D.; Ming, L.; Mei, H. Non-Contact Psychological Stress Detection Combining Heart Rate Variability and Facial Expressions. *Acta Opt. Sin.* **2021**, *41*, 68–77. [CrossRef]
- 19. Wang, M.; Jiang, R.-H.; Zhu, H. A review and revelation of the study of visual in human geography. *Hum. Geogr.* **2017**, 32, 10–19. [CrossRef]
- 20. Zhu, D. Theories, techniques and applied researches about eye-movement psychology. J. Nanjing Norm. Univ. Soc. Sci. Ed. 2005, 1, 90–95.
- 21. Liu, L.H.; Wu, M.Y.; Ma, Y.M.; Qu, H.Y. A Review of Eye Tracking Researches in Landscape Architecture Field. *J. Hum. Settl. West China* **2021**, *36*, 125–133. [CrossRef]

22. Sun, C.; Yang, Y. A study on visual saliency of way-finding landmarks based on eye-tracking experiments as exemplified in Harbin Kaide shopping center. *Archit. J.* **2019**, *605*, 18–23.

- 23. Wang, M.; Zhang, S.; Zhou, X. Campus environments and mental restoration: Eye-tracking evidence from dynamic stimuli. *Eng. Constr. Archit. Manag.* **2025**. [CrossRef]
- 24. Chen, Y.; Chen, Z.; Du, M. Designing Attention—Research on Landscape Experience Through Eye Tracking in Nanjing Road Pedestrian Mall (Street) in Shanghai. *Landsc. Archit. Front.* **2022**, *10*, 52–70. [CrossRef]
- 25. Zhu, S.; Du, S.; Li, Y.; Wei, S.; Jin, X.; Zhou, X.; Shi, X. A 3D spatiotemporal morphological database for urban green infrastructure and its applications. *Urban For. Urban Green.* **2021**, *58*, 126935. [CrossRef]
- 26. Xuan, S.; Wang, J.; Chen, Y. Reinforcement Learning for Stand Structure Optimization of Pinus yunnanensis Secondary Forests in Southwest China. *Forests* **2023**, *14*, 2456. [CrossRef]
- 27. Tsunetsugu, Y.; Park, B.J.; Ishii, H.; Hirano, H.; Kagawa, T.; Miyazaki, Y. Physiological effects of Shinrin-yoku (taking in the atmosphere of the forest) in an old-growth broadleaf forest in Yamagata Prefecture, Japan. *J. Physiol. Anthropol.* **2007**, 26, 135–142. [CrossRef] [PubMed]
- 28. Ren, Z.; Zhao, H.; Fu, Y.; Xiao, L.; Dong, Y. Effects of urban street trees on human thermal comfort and physiological indices: A case study in Changchun city, China. *J. For. Res.* **2022**, *33*, 911–922. [CrossRef]
- 29. Wang, T.-C.; Tsai, C.-L.; Tang, T.-W. Visual responses of patients with generalized anxiety disorder who cycling in the virtual sportscapes with different tree cover densities. *Front. Psychiatry* **2022**, *13*, 880586. [CrossRef]
- 30. Hosono, T.; Sato, S.; Wakabayashi, M.; Matsumoto, S. Physiological and Psychological Effects of Planting in Approach Areas of Rest Facilities on Highways. *Landsc. Stud. Online Proc.* **2017**, *10*, 31–36. [CrossRef]

**Disclaimer/Publisher's Note:** The statements, opinions and data contained in all publications are solely those of the individual author(s) and contributor(s) and not of MDPI and/or the editor(s). MDPI and/or the editor(s) disclaim responsibility for any injury to people or property resulting from any ideas, methods, instructions or products referred to in the content.